Progress In Electromagnetics Research M, Vol. 95, 199–209, 2020

Archimedean Spiral Antenna Loaded by Frequency Selective Surface

Jian-Yi Chu[1], Lin Peng[1, 2, *], Xiao-Feng Li[1], and Xing Jiang[1]

Abstract—A double-layer frequency selective surface (FSS) with dual rings is used as a reflector in the design of an Archimedean spiral antenna (ASA) with low radar cross section (RCS) and uni-directional characteristics. The proposed FSS presents a stopband in the range of 2 GHz to 4.7 GHz, which is applied to ASA to form a unidirectional radiation pattern with front to back ratio (FBR) values larger than 10 dB in the stopband, and the maximum FBR value is up to 25.26 dB. Compared with the reference antenna with the same-size metallic ground, the proposed FSS reduces the RCS about 2.5–38 dB in the frequency ranges of 4.8–30 GHz. And the FSS antenna also exhibits better axial ratio characteristics in the frequency range of 2.8–8.1 GHz. The composite structure is compact, with a total height of 0.18 wavelength at the lowest analysis frequency of 2 GHz. Measured results indicate that the proposed antenna reproduces the inherent wideband of the original ASA from 1.6 GHz to 8.1 GHz. Meanwhile, the gain of the ASA is increased by 3 dBi. Full-wave simulations and measurements prove that the novel FSS reflector can be employed to replace a metallic ground which realises a uni-directional ASA with broadband low RCS, high gain, and good circular polarization (CP) performance.

1. INTRODUCTION

It is known that the ASA operates as a wideband frequency-independent antenna which radiates CP beams with equal power in the upper and lower hemispheres spaces [1]. In many applications it is desired that the bidirectional pattern can be transformed to a uni-directional beam with a significant gain increase, when a back reflecting structure can be applied. Typically, a perfect electric conducting (PEC) ground plane can be applied to an ASA to obtain a uni-directional pattern, which should be $\lambda/4$ below the antenna to have constructive interferences. The fixed $\lambda/4$ distance means destructive interferences of incident and reflected waves at other frequencies, which seriously limits the frequency band [2]. To have a wide operating frequency band, an antenna can be backed by a cavity containing absorbing materials. However, a major disadvantage of this approach is that much of the radiated energy is dissipated in the absorber, which leads to low efficiency and gain [3]. Other techniques were also developed. The use of an electromagnetic band gap (EBG) plate [4] as a reflector results in a narrow band. The circularly symmetric high-impedance surface (HIS) [5] provides 16% operational bandwidths, and the gain of the spiral antenna is increased by 2.5 dBi compared to the antenna using a rectangular HIS. Therefore, by placing a HIS below the active regions of the ASA, the gain and front-to-back ratio (FBR) can be significantly improved [6]. A backing cavity composed of an FSS above a metal reflecting plate is designed to suppress the back lobe radiation and increase the gain of an ASA in [7]. The FSS is designed to reflect in the higher band (7–10 GHz) and transmit in the lower band (3–6 GHz). When the FSS and metal plate are inserted at a distance $\lambda/4$ below the spiral at the centre of the higher and lower bands, bidirectional to unidirectional beam transformation can be achieved. However, VSWR and axial ratio in the lower band are improved by means of inserting 560 Ω resistors at the end of the two arms.

Received 20 April 2020, Accepted 18 August 2020, Scheduled 28 August 2020

* Corresponding author: Lin Peng (penglin528@hotmail.com).

[1] Guangxi Key Laboratory of Wireless Wideband Communication and Signal Processing, Guilin University of Electronic Technology, Guilin, Guangxi 541004, China. [2] School of Physics, University of Electronic Science and Technology of China, Chengdu 610054, China.

In [8], a ring-shaped resonance-based reflector (RBR) was proposed to design a unidirectional antenna with low-profile and broadband characteristics. The RBR was composed of a metallic ring attached on a substrate, which achieved an in-phase reflection band ($-90^\circ < \phi < 90^\circ$) from 1.97 GHz to 4.94 GHz (85.96%). In [9], a director was applied to an RBR based antenna to enhance the FBR bandwidth, which would increase the profile. Although the RBR based antennas have very wide frequency band, their FRB bandwidth is not wide.

On the other hand, an antenna is also a high scattering object, which will make a high risk of interception by hostiles. Therefore, stealth technology to reduce the radar cross section (RCS) of an antenna system is important. Many techniques were proposed to reduce the RCS. Metamaterial absorber (MA) was applied to a waveguide slot antenna to reduce the RCS in [10]. An artificial magnetic conductor (AMC) is employed to replace the metallic ground of a slot antenna which produces broadband reflection cancellation to reduce RCS and enlarge the effective aperture simultaneously [11]. An RCS reduction of 6 dB is achieved from 4.34 to 7.16 GHz and 5.08 to 7.90 GHz, for the x-polarized and y-polarized incidences, respectively. By using the FSS ground instead of the solid metal ground, the RCS is reduced about 13–17 dB in the 3–10 GHz [12]. A novel switchable stacked artificial structure composed of an FSS and an MA is proposed in phased arrays to realize a smart integration of broadband RCS reduction and scanning range expansion in [13], and a 6 dB RCS reduction from 0.5 to 11.2 GHz for both TM and TE polarizations can be realized. A low-RCS and high-gain broadband circularly polarized (CP) antenna was designed using three kinds of artificial magnetic conductors arranged around the polarization conversion metasurface in [14]. The monostatic RCS of the antenna is reduced in a wide frequency band which depends on the reflection phase differences between the AMC and polarization conversion metasurface being 90°. The RCS of the proposed CP antenna in [14] is lower than that of the conventional CP antenna from 5 GHz to 10 GHz.

In this research, a double-layer concentric rings FSS is proposed and used in the design of a unidirectional and circular polarized ASA, while the RCS is also reduced in a very wide frequency band. By using a two ring structure, the FSS has a strong reflection in the 2 to 4.7 GHz band. The FBR values of the unidirectional ASA range from 2 GHz to 4.7 GHz with a standard of FBR $>$ 10 dB. Meanwhile, as the rings have the rotational symmetry, the FSS would be amicable to CP wave. The axial ratio (AR) of the proposed ASA is better than the ASA with PEC reflector, particularly in low frequency range. By using the FSS instead of the solid metal ground, the out-of-band RCS reduction can be realized in the frequency range of 4.8–30 GHz.

2. DESIGN AND ANALYSIS

2.1. Dual Ring Frequency Selective Surface

The unit cell of the FSS structure is shown in Fig. 1(a), and the proposed FSS consists of two concentric metal rings printed on two substrate layers with different radial lengths R_1 and R_2, respectively. The relative permittivity of the dielectric layers is 2.6, and the thickness is 1 mm. As a central symmetrical structure, the ring structure is suitable for circularly polarized antennas. The structure is simulated with unit cell boundary conditions on the four sides to model an infinite periodic structure and Floquet ports at the top and bottom sides as exhibited in Fig. 1(b). Fig. 1(c) demonstrates the reflection magnitudes and phases at surfaces of the single top and bottom rings. Fig. 1(d) presents the magnitudes and phases of the reflection coefficient as the unit cell and PEC are excited by a CP electromagnetic wave propagating in the $-z$-direction. From Fig. 1(c), the bottom ring and top ring resonate at 2.73 GHz and 4.19 GHz, respectively. It can be found from Fig. 1(d) that due to the combination of two rings, the wide stopband response range is obtained from 2 GHz to 4.7 GHz, and the reflection magnitude for the proposed FSS is reduced outside the stopband, which means that less energy of the incident wave is reflected. The incident wave within the stopband of the FSS will be reflected while the incident wave outside the stopband of the FSS will be transmitted through the FSS without any obstruction. Therefore, it can be used to reduce the RCS. The reflection phase of the perfect electric conductor (PEC) is invariably 180°. The reflection phase at the surface of the FSS is from 0° to 180°, which means that the phase is between the perfect magnetic conductor (PMC) (0°) and perfect electric conductor (PEC) (180°).

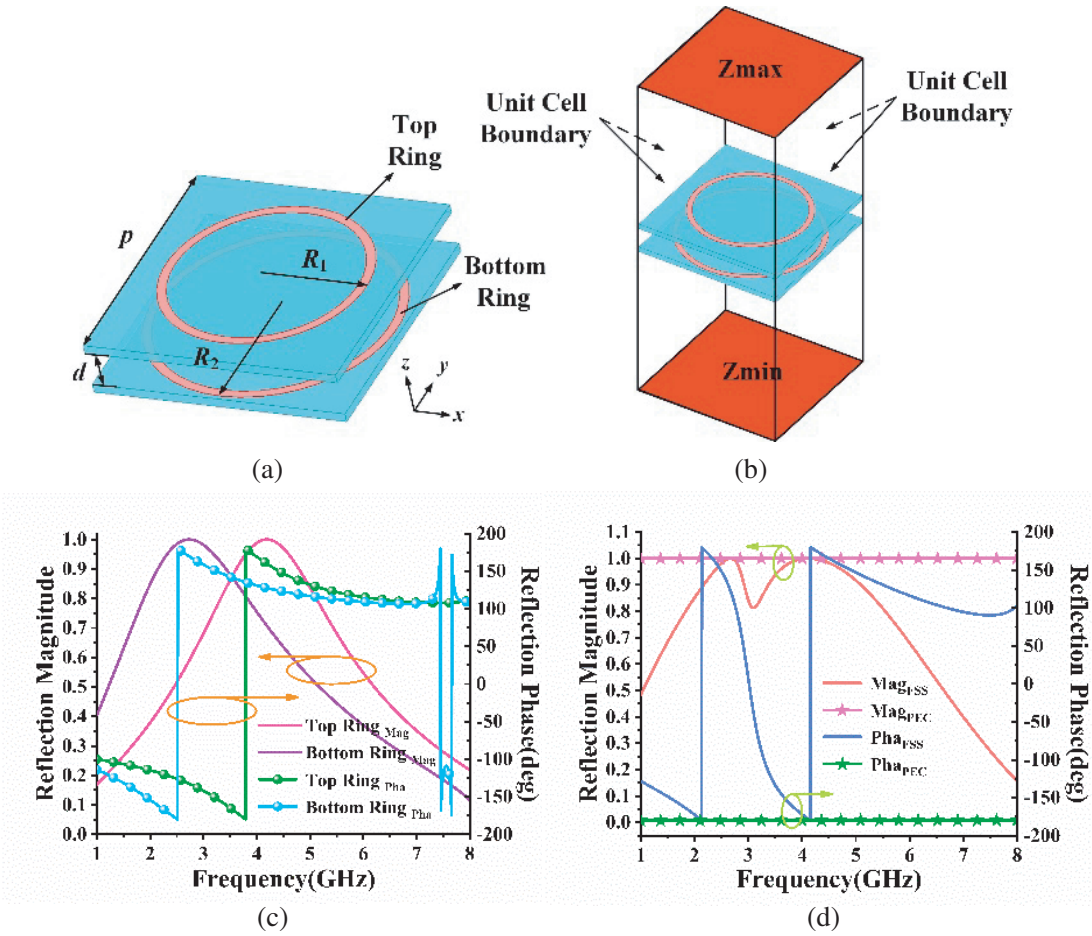

Figure 1. Unit cell structure of the proposed FSS. (a) 3D view. (b) Simulated model of the unit cell. (c) Reflection information of each ring. (d) Reflection information of the unit cell and PEC. ($p = 29$, $d = 4$, $R_1 = 11.5$, $R_2 = 14$) (unit: mm).

2.2. The ASA with the Frequency Selective Surface (ASAFSS) Design

A two-arm, three-turn ASA was designed as depicted in Fig. 2(a) with a loading ring to improve the AR characteristics at 2 GHz [15, 16]. The inner and outer diameters are 5 and 65 mm, respectively, and the distance between two adjacent arms and the width of the arms are approximately equal in order to achieve a self-complementary structure. The input impedance of the ASA is about 130 Ω, and the wide-band balun can transform the 130 Ω input impedance of the ASA to 50 Ω of an SMA connector. All parts of the design are printed on an F4B substrate with relative permittivity = 2.6, thickness = 1 mm, and loss tangent = 0.002. The antennas with the PEC reflector and FSS reflector are depicted in Figs. 2(b) and (c), respectively. They are denoted as ASA_{PEC} and ASA_{FSS}, respectively. Four cylindrical plastic posts with relative permittivity of $\varepsilon_r = 4$ are embedded between the ASA and reflectors to support the structures. The overall height (H_1) of the antenna is 27 mm. The FSS proposed in this paper is composed of 5×5 equal-sized lattices with a periodicity (p) of 29 mm. The PEC reflector has the same size.

The electric energy densities of the proposed ASA_{FSS} at three frequency points (2.6 GHz, 3.2 GHz, and 4.2 GHz) are plotted in Fig. 3. Note that 2.6 GHz and 4.2 GHz are the resonant frequencies of the large bottom ring and small top ring, respectively, while 3.2 GHz is located between resonances. From Figs. 3(a) and (c), the electric energy of 2.6 GHz concentrates at the large bottom ring layer of the FSS, while the electric energy of 4.2 GHz is gathered around the small top ring layer, which means that the electromagnetic waves at low frequencies are reflected by the large bottom ring layer, the

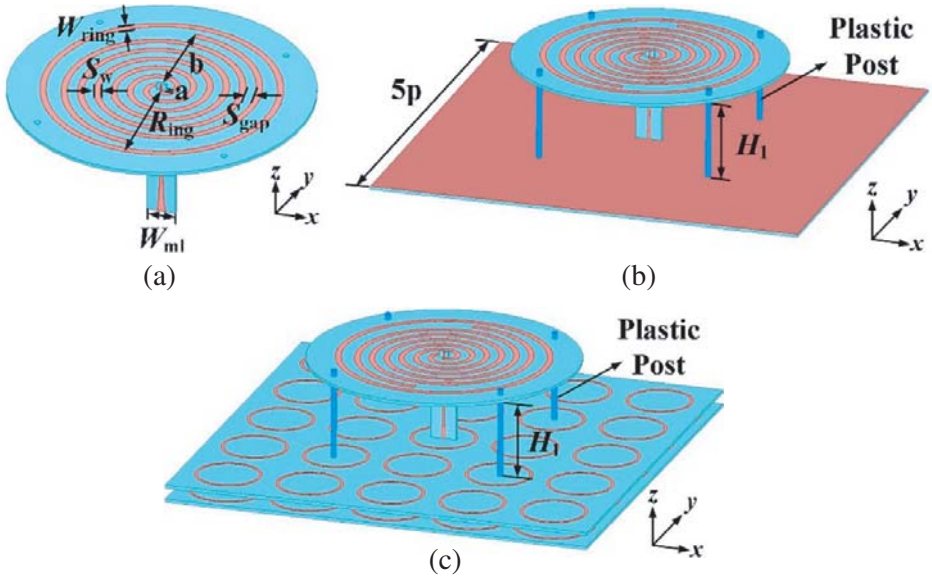

Figure 2. Geometry of the spiral antenna. (a) ASA. (b) ASA_{PEC}. (c) ASA_{FSS}. ($a = 1$, $b = 32$, $S_w = 2$, $S_{gap} = 2.5$, $W_{ring} = 2$, $R_{ring} = 35$, $H_1 = 27$) (unit: mm).

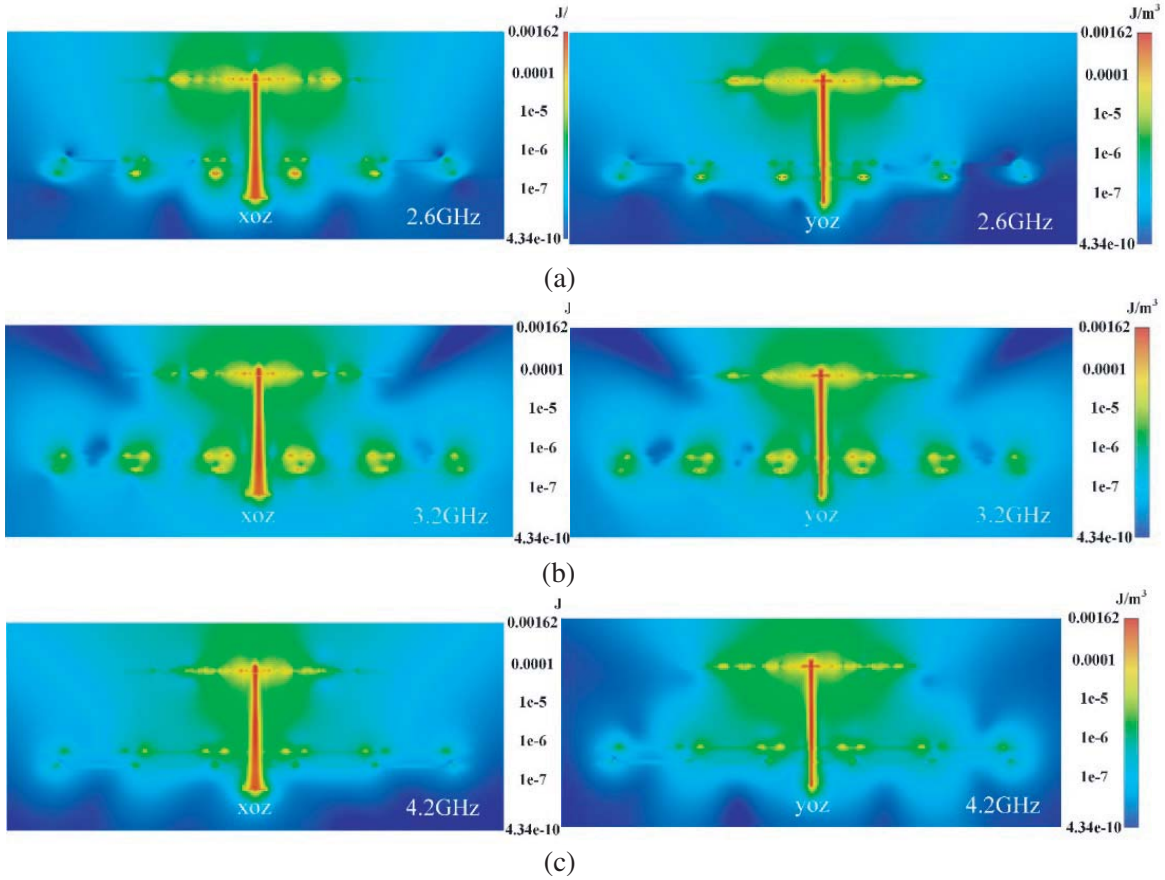

Figure 3. The electric energy densities of the proposed ASA_{FSS} at different frequency points. (a) 2.6 GHz. (b) 3.2 GHz. (c)4.2 GHz.

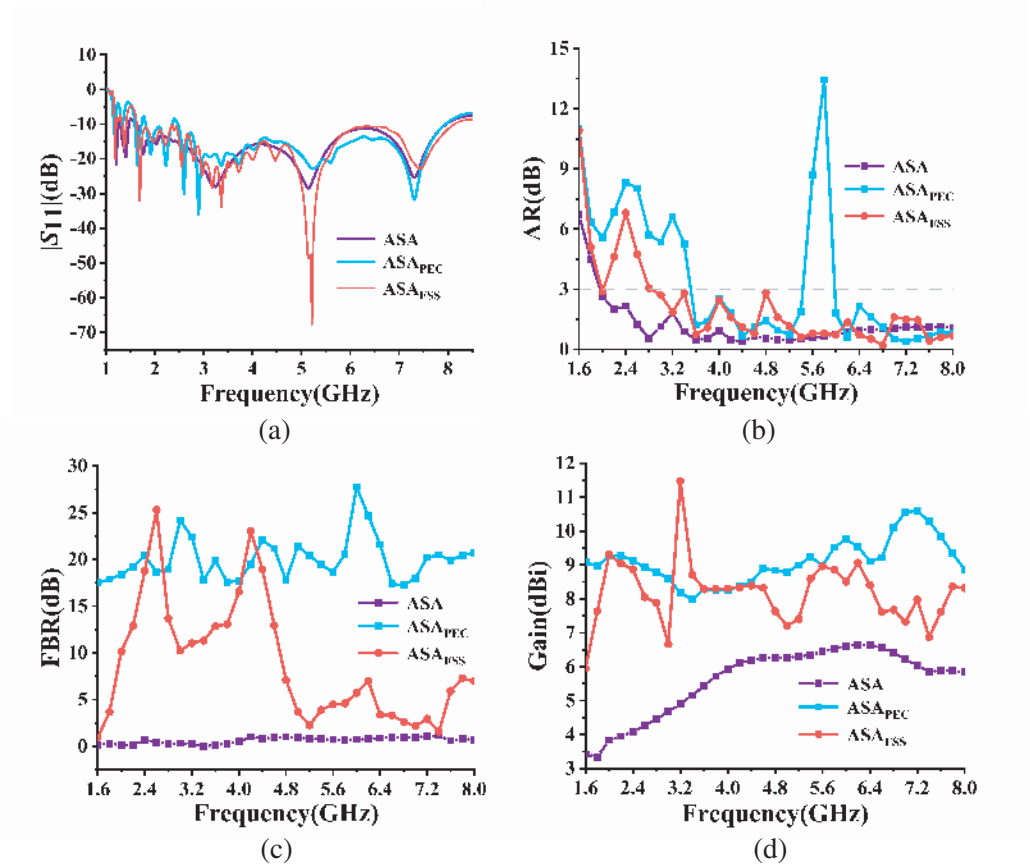

Figure 4. Comparisons of different antennas' performance. (a) $|S_{11}|$. (b) AR. (c) FBR. (d) gain.

electromagnetic waves at high frequencies are reflected by the small top layers, and the bi-directional radiation patterns are transformed to be uni-directional. From Fig. 3(b), the electric energy of 3.2 GHz is mainly distributed on both the ring layers. It is also interesting to find that compared to 2.6 GHz and 4.2 GHz, the electric energy of 3.2 GHz is spread out on the whole FSS structure. Therefore, the effective size at 3.2 GHz is much larger than that at other frequencies, which means that high gain could be obtained at 3.2 GHz.

The results of the proposed ASA_{FSS} are demonstrated in Fig. 4. Fig. 4(a) depicts the simulated $|S_{11}|$ curves of the antennas. As shown in the figure, all of the three antennas have good impedance matching characteristics from 1.6 GHz to 8.1 GHz. However, as shown in Fig. 4(b), the PEC reflector deteriorates the AR for the frequencies below 3.5 GHz. While the FSS based antenna has better AR, its AR is better than 3 dB for frequencies larger than 2.8 GHz. Besides, the AR at 5.6 GHz of ASA_{PEC} increases significantly, and it may be because profile height H_1 is approximately equal to half wavelength at 5.6 GHz. The 180° reflecting phase of the PEC reflector makes destructive interference between the reflected and radiating waves, while ASA_{FSS} does not have such a problem as the reflecting phase of the FSS is not 180° at 5.6 GHz. From Fig. 4(c), the FBR bandwidth of ASA_{FSS} ranges from 2 GHz to 4.7 GHz for FBR $>$ 10 dB, and it is within the stopband of the FSS. Note that the frequencies corresponding to the maximum FBR values are very close to the resonant frequencies of the two rings, while the FBR of the ASA_{PEC} is very large in the whole band. Then, it is expected that the ASA_{FSS} has better RCS than the ASA_{PEC} for high frequencies. From Fig. 4(d), the antennas with a reflector show greatly improved gain in the operating band. An increased peak gain of 11.5 dBi is observed at 3.2 GHz. This is because of the increased effective radiating aperture at 3.2 GHz as discussed in Fig. 3(b).

The RCS curves versus frequency for a normal incident CP plane wave are plotted in Fig. 5(a). The ASA_{FSS} has a range of 2.5–38 dB RCS reduction compared to the ASA_{PEC} in the frequency range

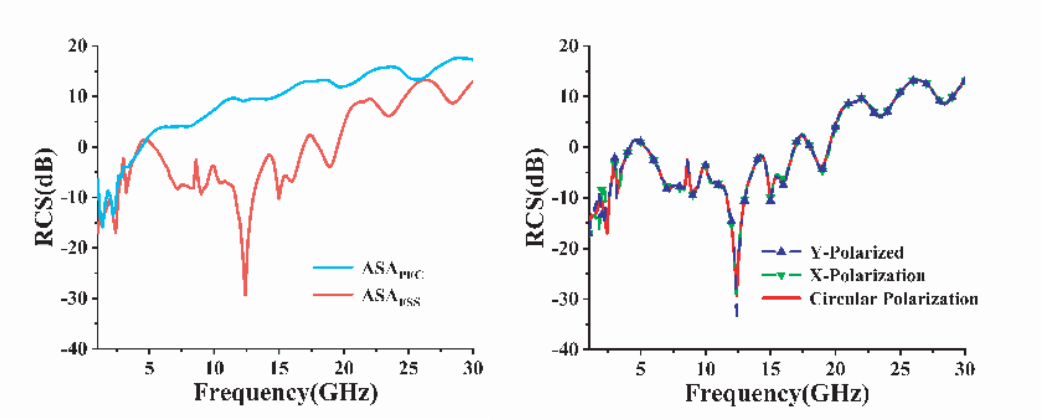

Figure 5. Simulated RCS versus frequency. (a) RCS of the antennas with CP incidence. (b) ASA_{FSS} under different polarization plane waves illumination.

of 4.8–30 GHz. Fig. 5(b) plots the simulated RCS of ASA_{FSS} under different polarization plane wave incidences. It is found that the RCS characteristics of the ASA_{FSS} are nonsensitive to the polarization state of the incident wave.

In order to reveal the uni-directional radiating characteristics of the ASA_{FSS}, the radiation patterns are depicted in Fig. 6. The figures are plotted at the $\varphi = 0°$ and $\varphi = 90°$ planes of 2.6, 3.2, and 4.2 GHz. From the figures, the ASA exhibits bidirectional radiation at all the frequencies with equal gain in the forward and back hemispheres, while the back lobes of the ASA_{FSS} and ASA_{PEC} are suppressed,

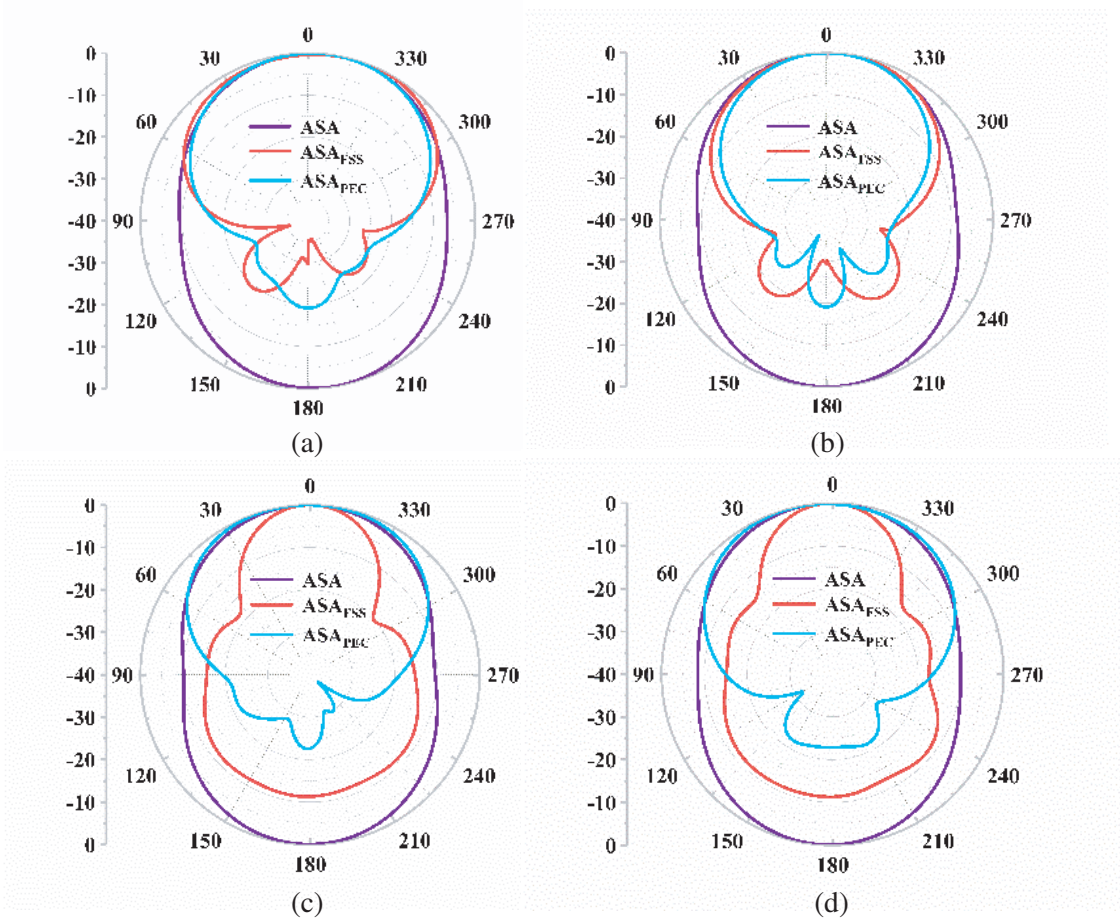

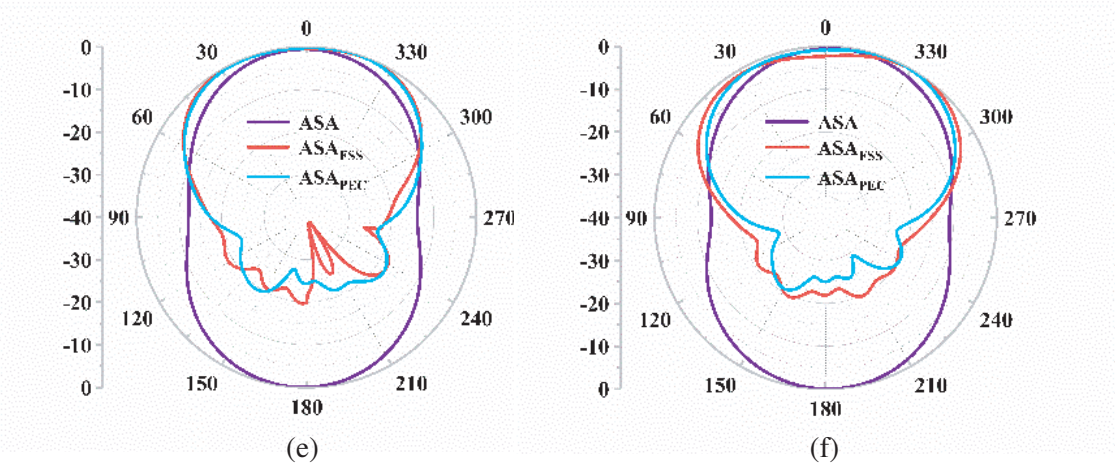

Figure 6. Normalized radiation pattern of different antennas. (a) 2.6 GHz at $\varphi = 0°$ plane. (b) 2.6 GHz at $\varphi = 90°$ plane. (c) 3.2 GHz at $\varphi = 0°$ plane. (d) 3.2 GHz at $\varphi = 90°$ plane. (e) 4.2 GHz at $\varphi = 0°$ plane. (f) 4.2 GHz at $\varphi = 90°$ plane.

and the antennas are uni-directional. As can be seen from Figs. 6(c) and 6(d), though the backward radiation of the ASA_{FSS} is larger than the ASA_{PEC} at 3.2 GHz, the FBR of ASA_{FSS} is still more than 10 dB. Moreover, the beamwidth of ASA_{FSS} at 3.2 GHz is narrower than that at other frequencies which results in a high gain.

3. FABRICATION AND MEASUREMENT

To validate the proposed design, the ASA_{FSS} prototype is fabricated and measured as shown in Fig. 7. The reflection coefficient of the proposed ASA_{FSS} is measured using a vector network analyzer (AV3656B) produced by China Electronics Technology Group Corporation (CETC)'s 41st Research Institute. The AR, FBR, and gain are measured. The gain is obtained from the measured S_{21} of two identical ASA_{FSS} and calculated by the Friis transmission equation. The radiation patterns were measured in a microwave chamber with NSI2000 nearfield system, while the RCS is also measured in the microwave chamber with two horn antennas as receiver and transmitter. Therefore, the RCS is measured with linear polarization incidence, and the RCSs of the linear and circular polarizations are almost the same from Fig. 5(b).

As shown in Fig. 8(a), the measured 10 dB impedance bandwidth is 136.6% with respect to the centre frequency of 5.05 GHz (1.6–8.5 GHz). The measured 3 dB AR bandwidth is 88.3% (3.1–8.0 GHz), whereas the simulated results are 96.3% (2.8–8 GHz) as shown in Fig. 8(b). Fig. 8(c) shows the simulated and measured FBR curves which are defined as the ratio of the front radiation (0°) to the back radiation (180°), and the measured FBR has reasonable agreement with the simulated one. The simulated and

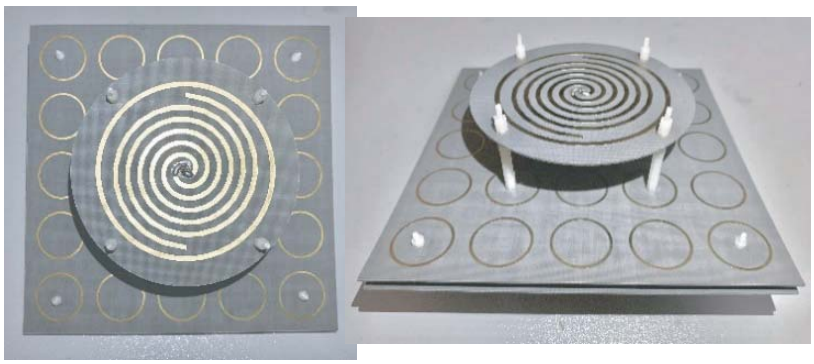

(a) (b)

(c) (d)

Figure 7. Photograph of fabricated ASA_{FSS} prototype. (a) Top view. (b) 3D view. (c) Manufactured prototype and measurement. (d) RCS measurement setup.

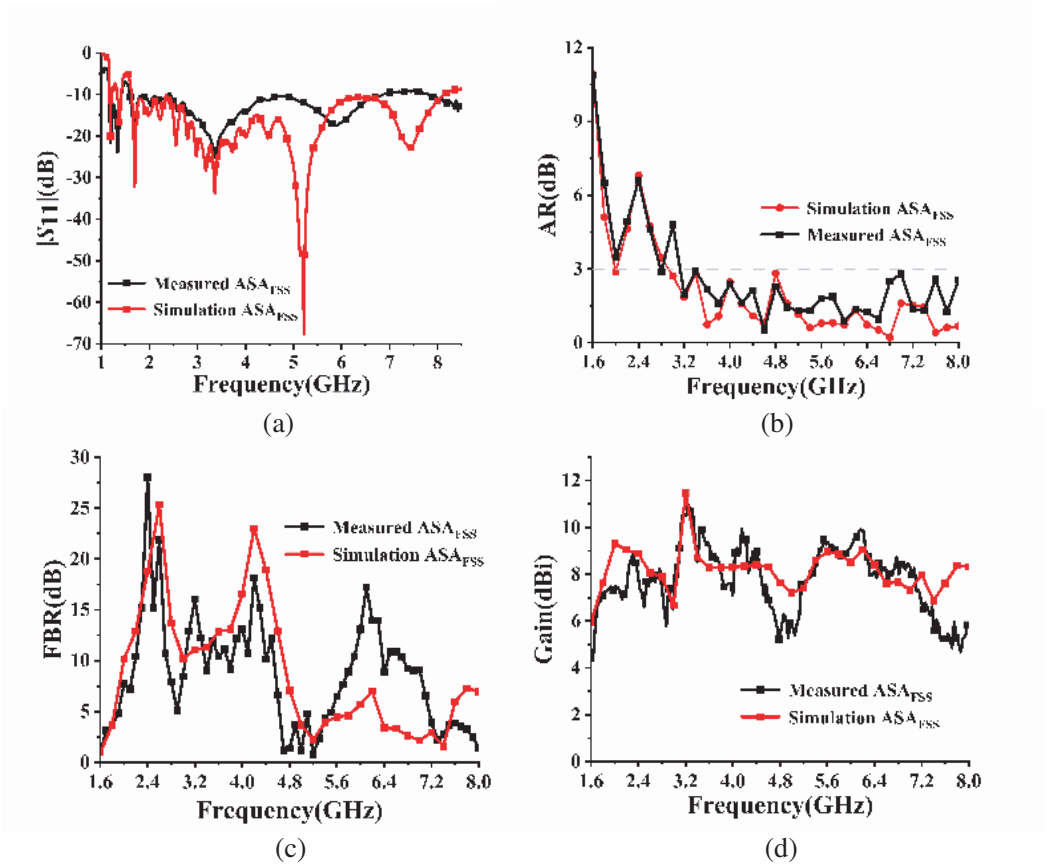

Figure 8. Comparison between simulation and measurement. (a) $|S_{11}|$. (b) AR. (c) FBR. (d) gain.

measured gain curves of the proposed ASA_{FSS} are plotted in Fig. 8(d). The measured gain also shows reasonable agreement with simulated one.

The RCS measurement setup is shown in Fig. 7(d), and the measured results are plotted in Fig. 9. Because of the clutter jamming of test environment and the noise of the hardware equipment such as the vector network analyzer, the measured S_{21} curves are jittery as demonstrated in Fig. 9(a). The measured data are denoised by wavelet analysis. The measured RCS results are calculated from the denoising S_{21} curves. By comparing with the denoising S_{21} of PEC ground, the RCS results of the proposed antenna under normal incidence with horizontal polarization are calculated by the radar equation. Although

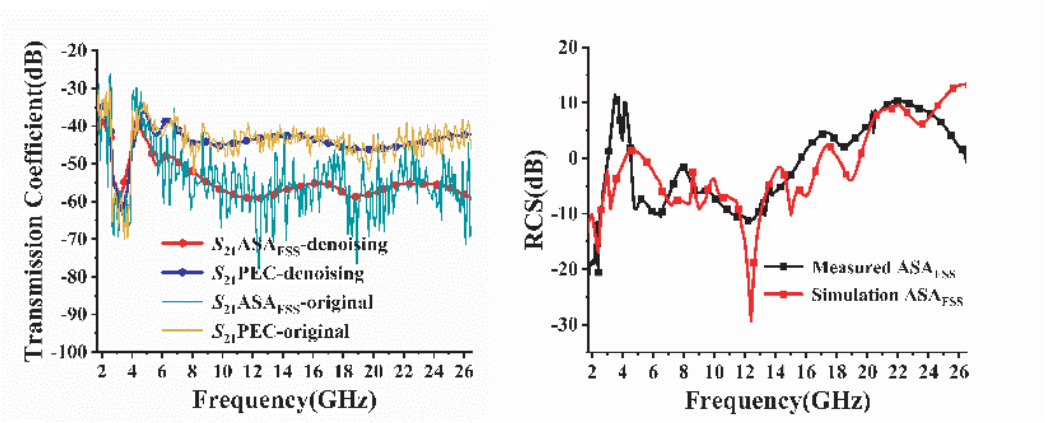

Figure 9. Measured results of the ASA_{FSS} and ASA_{PEC}. (a) Transmission coefficients between the horn antennas. (b) RCS.

there are some discrepancies between the simulated and measured results, they are attributed to the fabrication and test tolerances. The simulated and measured results show reasonable agreement, and the expected RCS reduction is obtained from Fig. 9(b).

The measured patterns of 2.6, 3.2, and 4.2 GHz are demonstrated in Fig. 10, and the simulated patterns are also plotted in the figure for comparison. Due to the limitations of the measurement environment, only a half of the space can be measured at a time; therefore, the front pattern and back pattern are measured separately and are combined to form the entire radiation pattern. Although

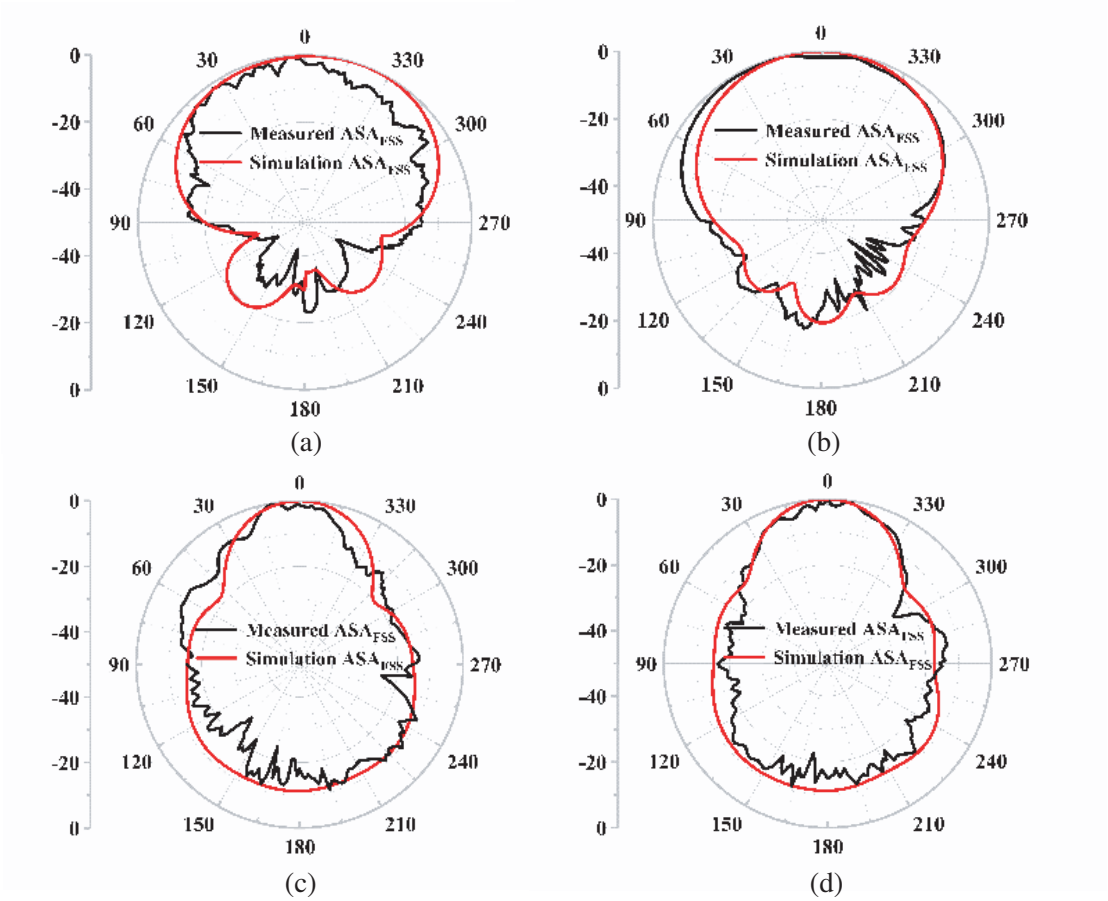

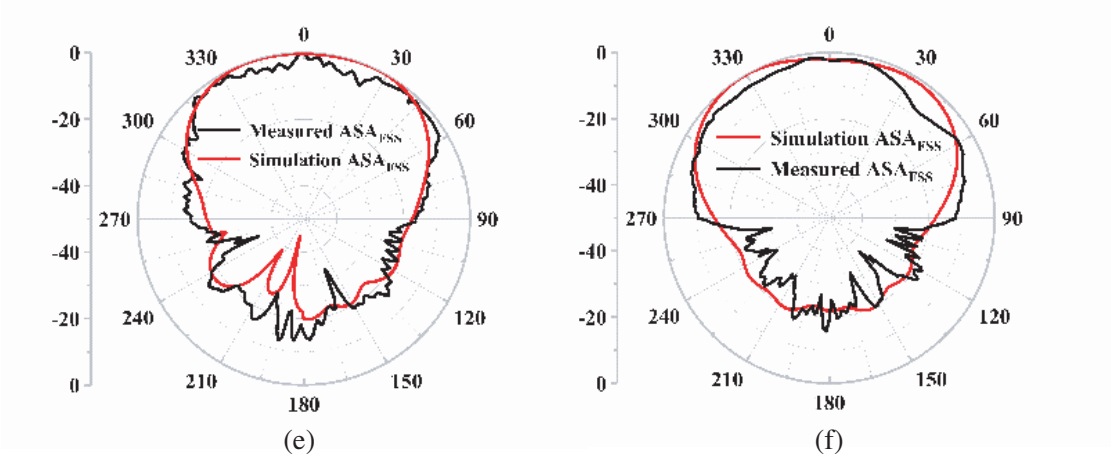

Figure 10. Normalized simulated and measured radiation patterns of the ASA_{FSS}. (a) 2.6 GHz at $\varphi = 0°$ plane. (b) 2.6 GHz at $\varphi = 90°$ plane. (c) 3.2 GHz at $\varphi = 0°$ plane. (d) 3.2 GHz at $\varphi = 90°$ plane. (e) 4.2 GHz at $\varphi = 0°$ plane. (f) 4.2 GHz at $\varphi = 90°$ plane.

discrepancies between the simulated and measured results are observed, both the simulation and measurement have verified good unidirectional patterns.

4. CONCLUSION

In this research, an FSS is used as a reflector to transform the bi-directional patterns of an ASA to be uni-directional and to realize low RCS. The concentric rings structure of the FSS makes a good circularly polarized characteristic for the proposed antenna. RCS reduction is achieved in a very wide frequency range of 4.8–30 GHz. With these outstanding features, the proposed antenna can be employed in wireless communication and radar stealth field.

ACKNOWLEDGMENT

This work was supported in part by the National Natural Science Foundation of China under Grant Nos. 61661011 & 61761012, in part by China Postdoctoral Science Foundation under Grant No. 2019M653371, and in part by Key Laboratory of Cognitive Radio and Information Processing, Ministry of Education (Guilin University of Electronic Technology) under Grant No. CRKL190101.

REFERENCES

1. Jia, Y. T., Y. Liu, S. X. Gong, W. B. Zhang, and G. S. Liao, "A low-RCS and high-gain circularly polarized antenna with a low profile," *IEEE Antennas Wireless Propag. Lett.*, Vol. 16, 2477–2480, 2017.
2. Stutzman, W. L. and G. A. Thiele, *Antennas Theory and Design*, Wiley, New York, 1981.
3. Nakano, H., S. Sasaki, H. Oyanagi, and J. Yamauchi, "Cavity-backed archimedean spiral antenna with strip absorber," *IET Microw. Antennas Propag.*, Vol. 2, No. 7, 725–730, Oct. 2008.
4. Bell, J. and M. Iskander, "A low-profile archimedean spiral antenna using an EBG ground plane," *IEEE Antennas Wireless Propag. Lett.*, Vol. 3, 223–226, 2004.
5. Amiri, M. A., C. A. Balanis, and C. R. Birtcher, "Gain and bandwidth enhancement of a spiral antenna using a circularly symmetric HIS," *IEEE Antennas Wireless Propag. Lett.*, Vol. 16, 1080–1083, 2017.
6. Mohamad, S., R. Cahill, and V. Fusco, "Selective high impedance surface active region loading of Archimedean spiral antenna," *IEEE Antennas Wireless Propag. Lett.*, Vol. 13, 810–813, 2014.

7. Mohamad, S., R. Cahill, and V. Fusco, "Performance of archimedean spiral antenna backed by FSS reflector," *Electron. Lett.*, Vol. 51, No. 1, 14–16, 2015.
8. Peng, L., J. Y. Xie, K. Sun, X. Jiang, and S. M. Li, "Resonance-based reflector and its application in unidirectional antenna with low-profile and broadband characteristics for wireless applications," *Sensors*, Vol. 16, No. 12, 2092-1–2092-14, 2016.
9. Peng, L., J. Y. Xie, X. F. Li, and X. Jiang, "Front to back ratio bandwidth enhancement of resonance based reflector antenna by using a ring-shape director and its time-domain analysis," *IEEE Access*, Vol. 5, 15318–15325, Jul. 2017.
10. Liu, T., X. Y. Cao, J. Gao, Q. R. Zheng, W. Q. Li, and H. H. Yang, "RCS reduction of waveguide slot antenna with metamaterial absorber," *IEEE Trans. Antennas Propag.*, Vol. 61, No. 3, 1479–1484, Mar. 2013.
11. Zhao, Y., X. Y. Cao, J. Gao, X. Yao, and X. Liu, "A low-RCS and high-gain slot antenna using broadband metasurface," *IEEE Antennas Wireless Propag. Lett.*, Vol. 15, 290–293, 2016.
12. Liu, Y., Y. W. Hao, H. Wang, K. Li, and S. X. Gong, "Low RCS microstrip patch antenna using requency-selective surface and microstrip resonator," *IEEE Antennas Wireless Propag. Lett.*, Vol. 14, 1290–1293, 2015.
13. Ding, X., Y. F. Cheng, W. Shao, and B. Z. Wang, "Broadband low-RCS phased array with wide-angle scanning performance based on the switchable stacked artificial structure," *IEEE Trans. Antennas Propag.*, Vol. 67, No. 10, 6452–6460, 2019.
14. Jia, Y. T., Y. Liu, S. X. Gong, W. B. Zhang, and G. S. Liao, "A low-RCS and high-gain circularly polarized antenna with a low profile," *IEEE Antennas Wireless Propag. Lett.*, Vol. 16, 2447–2480, 2017.
15. Liu, Q., C. L. Ruan, L. Peng, and W. X. Wu, "A novel compact archimedean spiral antenna with gap-loading," *Progress In Electromagnetics Research Letters*, Vol. 3, 169–177, 2008.
16. Peng, L., K. Sun, J. Y. Xie, Y. J. Qiu, and X. Jiang, "UWB bi-directional bow-tie antenna loaded by rings," *Journal of the Korean Physical Society*, Vol. 69, No. 1, 22–30, Jul. 2016.